

Skyrmion Lattice in Two-Dimensional Chiral Magnet

Jung Hoon Han,¹ Jiadong Zang,^{2,3} Zhihua Yang,¹ Jin-Hong Park,¹ and Naoto Nagaosa^{3,4}

¹*Department of Physics, BK21 Physics Research Division,
Sungkyunkwan University, Suwon 440-746, Korea*

²*Department of Physics, Fudan University, Shanghai 200433, China*

³*Department of Applied Physics, University of Tokyo,
7-3-1, Hongo, Bunkyo-ku, Tokyo 113-8656, Japan*

⁴*Cross-Correlated Materials Research Group (CMRG),
and Correlated Electron Research Group (CERG), RIKEN-ASI, Wako, Saitama 351-0198, Japan*
(Dated: November 26, 2024)

We develop a theory of the magnetic field-induced formation of Skyrmion crystal state in chiral magnets in two spatial dimensions, motivated by the recent discovery of the Skyrmionic phase of magnetization in thin film of $\text{Fe}_{0.5}\text{Co}_{0.5}\text{Si}$ and in the A-phase of MnSi . Ginzburg-Landau functional of the chiral magnet re-written in the CP^1 representation is shown to be a convenient framework for the analysis of the Skyrmion states. Phase diagram of the model at zero temperature gives a sequence of ground states, helical spin \rightarrow Skyrme crystal \rightarrow ferromagnet, as the external field B increases, in good accord with the thin-film experiment. In close analogy with Abrikosov's derivation of the vortex lattice solution in type-II superconductor, the CP^1 mean-field equation is solved and shown to reproduce the Skyrmion crystal state.

PACS numbers:

I. INTRODUCTION

Skyrmions, originally proposed as a model for baryons in nuclear physics¹, were first realized experimentally in the condensed-matter system of quantum Hall ferromagnets near integer filling factor $\nu \approx 1^{2,3}$. The electrons spontaneously form a fully polarized ferromagnet at $\nu = 1$ due to the exchange interaction, while slightly away from it the spins of extra (or lack thereof) electrons organize themselves into an intricate Skyrmionic structure as a result of the competitive interplay between the Zeeman and the Coulomb interactions². It was further suggested that these Skyrmions may condense into a crystalline form⁴. Skyrmions as quasiparticle excitations in quantum Hall ferromagnets are by now well established experimentally³. Recent experiments also find support for the crystallization of Skyrmions in the quantum Hall system⁵.

More recently, a strong case for the formation of Skyrme crystal (SkX) state was presented in the A-phase of a metallic ferromagnet MnSi ⁶ and other compounds of B20 structure^{7,8}. Here, the main evidence comes from small angle neutron diffraction data which exhibits a clear hexagonal pattern consistent with the triangular lattice arrangement of Skyrmions. Subsequent observation of the anomalous Hall effect in the A-phase gives additional support to the Skyrmion lattice picture⁹. On the other hand, Monte Carlo simulation of the two-dimensional classical spin model with the Dzyaloshinskii-Moriya (DM) interaction and magnetic anisotropy predicted the existence of various Skyrmion crystal phases as the ground state¹⁰. Just after this theoretical proposal, a real-space observation of the Skyrmions forming a crystalline phase has been provided by the Lorentz TEM imaging technique in the thin film of a non-

centrosymmetric magnetic crystal $\text{Fe}_{0.5}\text{Co}_{0.5}\text{Si}$ under a perpendicular magnetic field¹¹. By now there is accumulating experimental evidence stating that Skyrmion lattice is a natural occurrence in magnetic metals lacking inversion symmetry. For such crystals the role of the DM interaction is to convert a $\mathbf{k} = \mathbf{0}$ ferromagnetic ground state to a helical phase at a finite ordering vector, $\mathbf{k} \neq \mathbf{0}$, with the magnitude $|\mathbf{k}|$ fixed by the ratio of the DM exchange over the Heisenberg exchange energies. Influence of thermal fluctuation and/or the magnetic field can favor the formation of multiple spiral phase over a single spiral (In this paper we use the words “spiral” and “helical” interchangeably). When imaged in real space, the multiple spiral phase is none other than the Skyrmion lattice^{6,10,11}.

We should emphasize the contrasting behavior of the chiral magnet realized in two (2D) and three (3D) spatial dimensions. For 3D systems such as examined in Refs. 6–8, the Skyrmion crystal forms over a small window of finite temperature just below the paramagnetic transition known as the A-phase. On the other hand, for quasi-2D chiral magnets recently synthesized with the thickness smaller than a single spiral period¹¹, the Skyrmion phase occurs over a much larger temperature range extending nearly up to the paramagnetic transition and down to the lowest temperature measured, $T \approx 5\text{K}$, strongly suggesting that the Skyrme crystal is the ground state. Free energy analysis of the 3D model indeed shows stability of the Skyrmion phase at a finite temperature, but not at zero temperature^{6–8}. As shown in this paper, the 2D case supports the Skyrmion phase even at zero temperature.

Bogdanov and collaborators had earlier investigated the instability of the helical spin state to the spontaneous creation of Skyrmionic spin texture due to magnetic field in chiral magnets^{12,13}. Although not explicitly empha-

sized at that time, present experimental situation^{6-8,11} shows that the dimensionality plays a great role in stabilizing Skyrme crystal phase at low temperature. Our paper therefore re-visits the issue of the phase diagram of the chiral magnet under the influence of magnetic field first pioneered by Bogdanov *et al*, in light of these recent developments. We base our calculation explicitly on two dimensions, assuming spin models with zero spin anisotropy such as known to be the case for $\text{Fe}_{0.5}\text{Co}_{0.5}\text{Si}$. As a theoretical advance, we show that the Ginzburg-Landau action for the chiral magnet can be cast in a simple form using the CP^1 representation of the classical spin. The advantage offered by the new representation becomes evident when we consider the lattice case, where it becomes possible to derive the solution for the Skyrme lattice state by exploiting the analogy to another celebrated example of the lattice of topological defects - Abrikosov vortex lattice.

This paper is organized as follows. In Sec. II we introduce CP^1 formulation of the Ginzburg-Landau (GL) energy functional for a chiral magnet. In Sec. III we derive the zero-temperature phase diagram of the 2D chiral GL model using two complementary approaches. Both lead to the ground state evolution with the external field in excellent accord with the recent experiment. Analytical solution of the Skyrme lattice state is presented. Finally we conclude with a brief, qualitative discussion of thermal fluctuation effects for the Skyrme crystal and summarize in Sec. IV. One can read this paper as a companion article to Ref. 11, where the experimental findings and Monte Carlo results were reported.

II. CP^1 FORMULATION OF CHIRAL GINZBURG-LANDAU THEORY

We are concerned in this paper with magnetic systems lacking an inversion symmetry such as MnSi and $\text{Fe}_{1-x}\text{Co}_x\text{Si}$, where the magnetic interactions are characterized by a ferromagnetic exchange J and a weaker, Dzyaloshinskii-Moriya coupling D . Hereafter, we take the length of a structural unit cell as unity. The competition of the two interactions leads to a helical spin ground state with the pitch vector of length $k = D/J$. The effective continuum theory for such chiral magnet is provided by the Ginzburg-Landau (GL) energy functional¹²⁻¹⁴

$$\mathcal{F}[\mathbf{n}] = \frac{J}{2} \sum_{\mu} (\partial_{\mu}\mathbf{n}) \cdot (\partial_{\mu}\mathbf{n}) + D\mathbf{n} \cdot \nabla \times \mathbf{n} - \mathbf{B} \cdot \mathbf{n}. \quad (1)$$

The non-linear σ -model given in the first part describes the excitation of a conventional ferromagnet while the second term gives the effect due to the DM exchange. As we are interested in the effectively two-dimensional chiral magnet such as recently synthesized with $\text{Fe}_{0.5}\text{Co}_{0.5}\text{Si}$ ¹¹, the spatial derivatives run over the two-dimensional plane, $\mu = x, y$. The total energy is the spatial integral of \mathcal{F} : $F[\mathbf{n}] = \int d^2\mathbf{r} \mathcal{F}[\mathbf{n}]$. It is also known

that spin anisotropy does not play an important role in $\text{Fe}_{0.5}\text{Co}_{0.5}\text{Si}$, which is therefore omitted from the theory.

According to the Monte Carlo simulation¹⁰ and also the recent experiment¹¹, the spiral spin states at $\mathbf{B} = 0$ is supplanted by the hexagonal packing of Skyrmions when \mathbf{B} oriented perpendicular to the thin film plane exceeds a certain strength, B_{c1} . At still higher field strength $B > B_{c2}$ the Skyrme crystal state gives way to fully polarized ferromagnet. Both transitions are first-order, as evidenced by the presence of the co-existence region around both B_{c1} and B_{c2} ¹¹. For the intermediate phase $B_{c1} < B < B_{c2}$ the triangular lattice of Skyrmions identified by the Lorentz TEM bears striking resemblance to the Abrikosov vortex array in type-II superconductors^{15,16}. In this paper we correctly reproduce the observed first-order transitions of magnetic phases under increasing magnetic field, by comparing the energies of the three candidate states: H (helical), SkX (Skyrme crystal), and FM (ferromagnetic).

Previous theoretical approaches^{6,12-14} were based on the $\text{O}(3)$ representation of the spin vector, $\mathbf{n} = (\sin\theta \cos\phi, \sin\theta \sin\phi, \cos\theta)$. In this work, we adopt instead a “complex” description in which \mathbf{n} is replaced by a pair of complex fields

$$\mathbf{z} = \begin{pmatrix} z_1 \\ z_2 \end{pmatrix} = \begin{pmatrix} e^{-i\phi} \cos(\theta/2) \\ \sin(\theta/2) \end{pmatrix}, \quad (2)$$

obeying the unit-modulus constraint $\mathbf{z}^\dagger \mathbf{z} = 1$ ¹⁷. Mapping to the spin vector is through $\mathbf{n} = \mathbf{z}^\dagger \boldsymbol{\sigma} \mathbf{z}$. A well-known identity allows the re-writing of the nonlinear sigma model in the CP^1 language (no sum on μ)¹⁷

$$\begin{aligned} \frac{1}{4}(\partial_{\mu}\mathbf{n}) \cdot (\partial_{\mu}\mathbf{n}) &= (\partial_{\mu}\mathbf{z}^\dagger) \cdot (\partial_{\mu}\mathbf{z}) - A_{\mu}^2, \\ A_{\mu} &= -\frac{i}{2}[\mathbf{z}^\dagger(\partial_{\mu}\mathbf{z}) - (\partial_{\mu}\mathbf{z}^\dagger)\mathbf{z}]. \end{aligned} \quad (3)$$

The Skyrme density is related to the magnetic field associated with the vector potential by $\frac{1}{2}\mathbf{n} \cdot (\partial_x \mathbf{n} \times \partial_y \mathbf{n}) = \partial_x A_y - \partial_y A_x$. The chiral, DM term in the energy (1) under the CP^1 mapping becomes

$$\mathbf{n} \cdot (\nabla \times \mathbf{n}) = -2\mathbf{n} \cdot \mathbf{A} - i\mathbf{z}^\dagger (\boldsymbol{\sigma} \cdot \nabla) \mathbf{z} + i(\nabla \mathbf{z}^\dagger) \cdot \boldsymbol{\sigma} \mathbf{z}. \quad (4)$$

When Eqs. (3) and (4) are combined, the energy density re-written in the CP^1 representation takes on a succinct form

$$\begin{aligned} \mathcal{F}[\mathbf{z}] &= 2J \sum_{\mu} \left(D_{\mu} \mathbf{z} \right)^\dagger \left(D_{\mu} \mathbf{z} \right) - \mathbf{B} \cdot \mathbf{z}^\dagger \boldsymbol{\sigma} \mathbf{z}, \\ D_{\mu} &= \partial_{\mu} - iA_{\mu} - i\kappa\sigma_{\mu}. \end{aligned} \quad (5)$$

The derivative D_{μ} is a 2×2 matrix due to the non-zero DM exchange, $\kappa = D/2J$. This CP^1 version of the energy density of a chiral magnet and the saddle-point equation which follows from it form the basis of the subsequent analysis¹⁸.

To orient the readers, we first discuss how to write down a conventional magnetic state in the CP^1 language. The ferromagnetic state for instance is written $\mathbf{z}_{\text{FM}} = \mathbf{z}_0$, an arbitrary constant spinor. The helical spin state - the ground state of Eq. (1) at zero magnetic field - is obtained from FM by a position(\mathbf{r})-dependent twist of the spin orientation,

$$\mathbf{z}_{\text{H}} = e^{i\kappa(\boldsymbol{\sigma} \cdot \hat{\mathbf{k}})(\mathbf{r} \cdot \hat{\mathbf{k}})} \mathbf{z}_0. \quad (6)$$

The Pauli matrix $\boldsymbol{\sigma}$ appears above. It can be checked that the associated spin configuration $\mathbf{n}_{\text{H}} = \mathbf{z}_{\text{H}}^\dagger \boldsymbol{\sigma} \mathbf{z}_{\text{H}}$ is indeed orthogonal to the propagation vector direction $\hat{\mathbf{k}} = \mathbf{k}/|\mathbf{k}|$ and rotates with the pitch $k = 2\kappa = D/J$, provided the initial spin orientation $\mathbf{n}_0 = \mathbf{z}_0^\dagger \boldsymbol{\sigma} \mathbf{z}_0$ is perpendicular to $\hat{\mathbf{k}}$. The vector potential \mathbf{A} for the helical spin state is identically zero.

An isolated Skyrmion in two dimensions with the spin pointing down at the origin $r = 0$ and up far away, $r \rightarrow \infty$, is given the CP^1 expression¹⁹

$$\mathbf{z}_{\text{Sk}} = e^{i(\theta(r)/2)(\boldsymbol{\sigma} \cdot \hat{\mathbf{r}} \times \hat{\mathbf{z}})} \mathbf{z}_0, \quad (7)$$

where $\mathbf{z}_0 = \begin{pmatrix} 1 \\ 0 \end{pmatrix}$, and $\hat{\mathbf{r}} = (\cos \varphi, \sin \varphi, 0)$ is the radial vector (We use ϕ for the azimuthal angle of the spin vector \mathbf{n} , and φ for the azimuthal angle of the coordinate $\mathbf{r} = (x, y)$: $\tan \varphi = y/x$). The polar angle $\theta(r)$ is a function of the radial coordinate r such that $\theta(0) = \pi$, $\theta(\infty) = 0$, and smoothly varying in between. Vector potential for the single-Skyrmion configuration is $\mathbf{A}_{\text{Sk}} = (\hat{\varphi}/r) \sin^2(\theta/2)$. As a concrete example of a single (anti-)Skyrmion one can take the following case,

$$n^z = \frac{r^2 - R^2}{r^2 + R^2}, \quad n^x + in^y = 2iR \frac{x + iy}{r^2 + R^2}, \quad (8)$$

and the associated CP^1 expression $\mathbf{z}_{\text{Sk}} = \frac{1}{\sqrt{R^2 + r^2}} \begin{pmatrix} ix + y \\ -R \end{pmatrix}$. Note that the z_1 part of the CP^1 Skyrmion solution behaves exactly as would a (anti-)vortex: depleted to zero at the core, winding about the origin as $\sim e^{-i\varphi}$, and reaching a constant unit magnitude when $r/R \gg 1$ (See Fig. 1). At least pictorially it is clear that U(1) vortex configuration in the CP^1 representation (in z_1 for instance) implies a Skyrmionic spin configuration in \mathbf{n} through the mapping $\mathbf{n} = \mathbf{z}^\dagger \boldsymbol{\sigma} \mathbf{z}$. In the next section, we will show that the mapping from a U(1) vortex to the real-spin Skyrmion can be extended to the lattice case as well.

The spin configuration Eq. (8) is the saddle point solution of the first, Heisenberg-only term of the free energy given in Eq. (1). It is an excited state, with the energy $E = 4\pi J$ independent of the radius of the Skyrmion R , and carrying a non-trivial topological number¹⁹. On the other hand, the Skyrmion state can become the *ground*

state if we consider the full free energy in Eq. (1). Although the exact spin configuration will be somewhat different from that given in Eq. (8), the topological properties remain the same. Furthermore, the radius R is uniquely determined by the ratio of DM interaction and the exchange energy as shown in the next section. For Skyrmions in the quantum Hall system the radius was fixed by the relative strengths of Zeeman and Coulomb interactions².

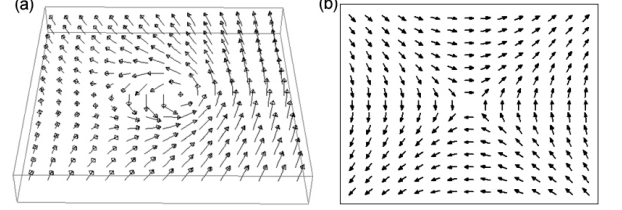


FIG. 1: (a) A typical (anti-)Skyrmion configuration given by Eq. (8) with $R = 2$. (b) z_1 component of the CP^1 Skyrmion \mathbf{z}_{Sk} . When expressed as a planar spin ($\text{Re}[z_1], \text{Im}[z_1]$), it is an anti-vortex.

III. PHASE DIAGRAM

In this section we address the phase diagram of the model, Eq. (1) or Eq. (5), as the external field $\mathbf{B} = B\hat{\mathbf{z}}$, always assumed to be in the positive z -direction ($B > 0$), increases from zero. Experimentally, the low-temperature phase evolves as helical spin, SkX, and FM with increasing field strength. We adopt two approaches for calculation of the energies of the respective phases, both of which successfully reproduce the observed phase evolution. In addition, we obtain analytic results for the two critical fields B_{c1} and B_{c2} ($B_{c1} < B_{c2}$), each referring to the first-order critical field separating H from SkX (B_{c1}), and SkX from FM (B_{c2}).

A. Variational analysis of a single Skyrmion

In this subsection, we regard the Skyrmion lattice as the close-packing of individual Skyrmions of radius R forming a triangular lattice. The local spin orientation (θ, ϕ) of a single Skyrmion depends on the local coordinate (r, φ) as $\phi = \varphi - \pi/2$ and $\theta = \theta(r)$. The total free energy of a single Skyrmion reads

$$F_{\text{Sk}} = 2J \int 2\pi r dr \left[\left(\frac{1}{2} \frac{d\theta}{dr} + \kappa \right)^2 - \kappa^2 + \frac{\kappa}{r} \sin \theta \cos \theta + \frac{1}{4r^2} \sin^2 \theta - \beta(\cos \theta - 1) \right], \quad (9)$$

where $\beta = B/(2J)$, and the FM state is chosen to have the free energy zero. Ferromagnetic configuration is enforced in the outermost region by the upward magnetic

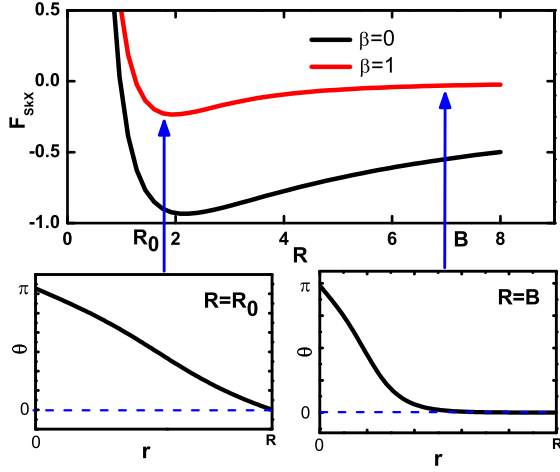


FIG. 2: (color online) Dependence of the free energy density F_{SkX} on the radical cutoff R at magnetic field $\beta = 1$ (red curve) and $\beta = 0$ (black curve), respectively. We choose $\kappa = 1$. The angle θ measured from the z -axis as a function of the distance r from the center of the Skyrmion for two different R 's are shown in the insets. Optimal R_0 for $\beta = 1$ leads to an almost linear dependence of $\theta(r)$ on r , while larger $R = B$ leads to a long ferromagnetic tail outside the Skyrmion core region with radius $\cong R_0$.

field, so that $\theta(\infty) = 0$. On the contrary, $\theta(0) = \pi$ due to the geometric nature of Skyrmion. In numerical calculations, a hard radical cutoff R is introduced such that $\theta(r) = 0$ for $r \geq R$. In physical terms R is half the inter-Skyrmion distance in the Skymre crystal. The Skyrmion lattice observed experimentally can be constructed as the close-packing of non-overlapping, individual Skyrmions in a triangular lattice. One can write down the total free energy of the Skymre crystal state as

$$F_{\text{SkX}} = \frac{L^2}{2\sqrt{3}R^2} F_{\text{Sk}}, \quad (10)$$

L being the sample size. For each cutoff R , we can apply the numerical variation to minimize the free energy F_{Sk} for a single Skyrmion. The equilibrium configuration of the whole lattice should minimize F_{SkX} , hence the free energy density functional $F_{\text{Sk}}[\theta(r)]/R^2$ by optimizing $\theta(r)$.

Figure 2 shows dependence of the free energy F_{SkX} on the cutoff R , where the sample size is normalized. It clearly shows that when R increases from zero, F_{SkX} decreases dramatically, and reaches a minimal value at R_0 . This point is exactly the ground state of the helical magnet at zero temperature where the compromise between Zeeman, Heisenberg and DM interactions are reached to the maximum degree. The configuration of $\theta(r)$ is shown in the left inset of Fig. 2. One can find that $\theta(r)$ varies almost linearly in the whole region from 0 to R_0 , and reaches zero at R_0 . In this case, R_0 defines both the

typical Skyrmion size as well as half of the optimal inter-Skyrmion distance, and the Skyrmions are close-packed. Applying the dimensional analysis to Eq. (9), one finds r has the same dimension as $1/\kappa \sim J/D$. Therefore it is expected that R_0 would be proportional to $1/\kappa$, which is confirmed numerically as well.

When the cutoff R exceeds the optimal distance R_0 , the free energy starts to increase from the negative minimal value and approaches zero as $R \rightarrow \infty$. From the corresponding configuration shown in the right inset of Fig. 2 one can see that at $R > R_0$, the variation of $\theta(r)$ is qualitatively different from that at $R = R_0$. A ferromagnetic tail with $\theta = 0$ appears over the region between R_0 and R . In usual conventions, only the core region where the variation in $\theta(r)$ is nonzero is referred as a Skyrmion. Therefore two neighboring Skyrmions are well-separated by the intervening FM phase in this case, and the Skyrmions are not close-packed.

The other competing phase observed besides the Skyrmion lattice is the spiral configuration at small magnetic field. This helical phase is the exact ground state of the Hamiltonian containing the DM interaction when the external field is absent. To see how the free energy of the helical state varies with field, consider the spiral spin propagating along y direction with $\phi = 0$ and $\theta = \theta(y)$ is a function of y . The free energy for half period of spiral is

$$F_{\text{H}} = \frac{2JL}{\ell} \int_0^\ell dy \left[\left(\frac{1}{2} \frac{d\theta}{dy} + \kappa \right)^2 - \kappa^2 - \beta(\cos \theta - 1) \right], \quad (11)$$

with the boundary condition $\theta(0) = \pi$ and $\theta(\ell) = 0$, where 2ℓ is the period of a spiral. Similar to the Skyrmion lattice case, one can derive the optimal ℓ by minimizing this free energy functional to get the configuration for a spiral lattice.

The free energies of the three phases (helical, SkX, FM) for $\kappa = 1$ obtained by variation are shown in Fig. 3. It is explicitly shown that the spiral state has the lowest energy among the three configurations when the external magnetic field is small. In the large field limit, ferromagnetism is energetically favored. In the intermediate region, one finds the Skyrmion phase as a compromise between the DM and Zeeman energies. This is because the Skyrmion configuration keeps the spiral structure inside and ferromagnetic state outside, and hence can gain both the DM energy and magnetic field energy. This result is quite consistent with the Monte Carlo simulation¹⁰ and the experiment¹¹. The lower (β_{c1}) and upper (β_{c2}) critical field strengths separating the Skyrmion phase from other phases can be easily determined by the intersects of Skyrmion energy line with the other two in Fig. 3. Applying dimensional analysis to Eq. (9) or Eq. (11), the normalized magnetic field β is found to have the same dimension as κ^2 . Therefore one expects both β_{c1} and β_{c2} to scale with κ^2 , a fact also established by numerical calculation. Restoring proper units, we get the two critical fields

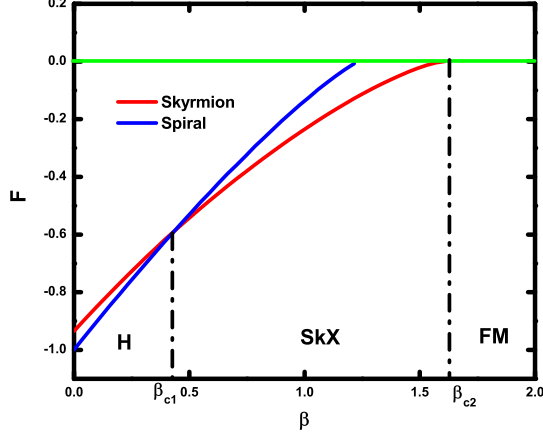


FIG. 3: (color online) The energies of the three states, i.e., (i) helical state, (ii) Skymion crystal, and (iii) ferromagnetic state. The free energy of ferromagnetic order is set to be zero, which is labeled in green. The helical state is energetically favored at low magnetic field, while the Skymion phase emerges at intermediate magnetic field. Ferromagnetism is favored at larger fields.

$$B_{c1} = 0.2D^2/J, \quad B_{c2} = 0.8D^2/J. \quad (12)$$

For $\text{Fe}_{0.5}\text{Co}_{0.5}\text{Si}$ thin film, the two critical fields at low temperatures were $B_{c1} \approx 40\text{mT}$ and $B_{c2} \approx 80\text{mT}$ ¹¹. Due to the co-existence region in the experimental phase diagram, it is not possible to pin down the critical fields more precisely. We can still make some estimates based on the above analytical formulas of the critical fields. The observed spiral wave length of 90nm and the unit cell size of $a \sim 4.5\text{\AA}$ gives the ratio $D/J = 2\pi(a/\lambda) \approx 1/30$. The critical fields are of order $D^2/J = J(D/J)^2 \sim J/900$. If we take the observed paramagnetic transition temperature of $\sim 30\text{K}$ as a measure of J , we would get $B_c \sim 30\text{K}/900 \sim (1/30)\text{K}$ which in magnetic field unit becomes $\sim (1/30)\text{T}$, in excellent agreement with the observe field ranges of 40-80 mT for the Skymion lattice. The criteria derived in Eq. (12) is general, applicable to a wide range of chiral magnets characterized by both J and D without the strong spin anisotropy effects. For such systems the Skyrme crystal phase formation is expected in the field range of D^2/J .

The phase diagram sheds light on the properties of phase transition as well. Two lines of spiral and SkX have different slopes at the critical field β_{c1} , as shown in Fig. 3. Therefore the phase transition between spiral and SkX phase is first order due to the discontinuity of $\partial F/\partial\beta$ across the phase boundary. For the transition from SkX to FM, we carefully examined the derivative $\partial F/\partial\beta$ of the SkX phase as shown in Fig. 4. At the critical field $\beta_{c2} = 1.6$, $\partial F/\partial\beta$ of SkX is clearly nonvanishing. However the free energy of the FM phase is set to be zero

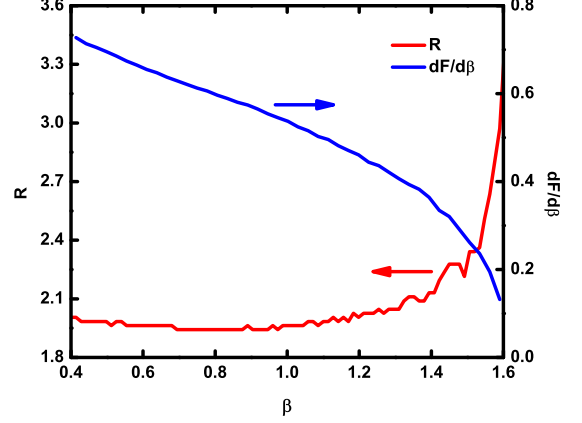


FIG. 4: (color online) The inter-Skymion distance in SkX (in red), and the first order derivative of SkX's free energy with respect to the magnetic field β (in blue). The distance increases rapidly near the transition from SkX to FM phase. As the derivative is nonvanishing at the critical field $\beta_{c2} = 1.6$, this transition is first order.

already, so $\partial F/\partial\beta = 0$ on the FM side. Consequently the transition between SkX and ferromagnetic phases is first order as well. This is quite consistent with the experimental results¹¹. Another interesting issue is the deformation of Skyrmions at the phase transition from SkX to FM. Half of the optimized inter-Skymion distance, denoted by R , in SkX is shown in Fig. 4. Deep inside the SkX phase, the inter-Skymion distance is roughly unchanged, which is just the optimal distance $2R_0$ controlled by the Dzyaloshinskii-Moriya physics as discussed above. However when the magnetic field approaches the critical value β_{c2} , the inter-Skymion distance increases very rapidly. In this situation, the configuration of the individual Skymion resembles the one shown in the right inset of Fig. 2. The ferromagnetic tail grows significantly while leaving the core region almost unchanged around radius R_0 . The growing FM tail near β_{c2} indicates that the Skyrmions are separated far away by the intervening FM phase, and become more and more dilute when the magnetic field approaches β_{c2} .

One should be careful to distinguish the SkX with $R \gg R_0$ from the FM state. In both states the average magnetization is fully saturated, but there is a qualitative difference in the two phases because of the existence of topological defects in the SkX. This explains why the SkX \rightarrow FM transition is still first-order (one cannot turn off topological defects smoothly), despite the fact that the magnetization reaches unity in a continuous manner at the SkX/FM phase boundary. A careful examination of the Skymion size and the inter-Skymion distance in the thin-film chiral magnet near the upper critical field is expected to confirm the field dependence of the two length scales R_0 and R discussed in this subsection.

B. Analogy to Abrikosov Lattice

In Sec. II, we briefly pointed out the vortex \leftrightarrow Skyrmion correspondence established by the CP^1 mapping (See Fig. 1). In this subsection, we argue that the correspondence in fact extends to the case of their respective lattice structures.

Abrikosov put forward the lattice solution of vortices in a type-II superconductor of the form¹⁵

$$\psi(x, y) = \sum_{j=-\infty}^{\infty} c_j e^{2\pi i(jy/l_y)} e^{-(x-jl_x)^2/2\xi^2}, \quad (13)$$

with some constants c_j . Here ξ is the correlation length, l_x, l_y are the inter-vortex separations in the x - and y -directions, respectively, with the relation $l_x l_y = h/eB = 2\pi l_B^2$, l_B =magnetic length. We now pose the question: can one construct a spinor solution $\mathbf{z}_{\text{SkX}}(x, y)$ in the same spirit as Abrikosov's vortex lattice solution, such that the associated spin configuration $\mathbf{n}_{\text{SkX}} = \mathbf{z}_{\text{SkX}}^\dagger \boldsymbol{\sigma} \mathbf{z}_{\text{SkX}}$ is the Skyrmion lattice?

We start by writing down the saddle-point equation derived by minimizing the total energy, E . The constraint $\mathbf{z}^\dagger \mathbf{z} = 1$ is implemented by augmenting the total energy with the Lagrange multiplier field $\lambda(\mathbf{r})$: $E \rightarrow H = E + \int d^2\mathbf{r} \lambda(\mathbf{z}^\dagger \mathbf{z} - 1)$. Taking the variational derivative $\delta H/\delta \mathbf{z}^\dagger = 0$ yields the saddle-point equation

$$2J(\nabla - i\mathbf{A} - i\kappa\boldsymbol{\sigma})^2 \mathbf{z} + 2iD(\mathbf{n} \cdot \nabla)\mathbf{z} + (\mathbf{B} \cdot \boldsymbol{\sigma})\mathbf{z} = \lambda\mathbf{z}. \quad (14)$$

As a self-consistency check, one can show that the helical spin solution (6) indeed satisfies the equation when $\mathbf{B} = 0$.

The Skyrme crystal state generates a non-zero Skyrmion number that translates into a non-zero effective magnetic field, $\partial_x A_y - \partial_y A_x \neq 0$, which in turn should generate a Landau-level-type solution. The actual equation is non-linear, however, and the underlying Landau level structure is not clear. The non-linearity arises from two sources. One is that the vector potential \mathbf{A} depends on the knowledge of the solution \mathbf{z} itself. The second is the presence of $2iD(\mathbf{n} \cdot \nabla)\mathbf{z}$ in the equation. In regard to the second issue we are reminded the fact that the SkX state exists under a finite magnetic field which partially polarize the spins. Numerical calculation shows that the mean moment in the SkX state can be a good fraction of the full moment¹⁰. It thus appears reasonable to take a spatial average of \mathbf{n} and obtain $\mathbf{n} \cdot \nabla \mathbf{z} \rightarrow \langle \mathbf{n} \rangle \cdot \nabla \mathbf{z} = 0$, since the spatial gradient in the two-dimensional lattice is orthogonal to the average moment direction along \hat{z} . Such a conclusion will not generally hold for 3D lattice or for field tilted away from the \hat{z} -direction in the 2D lattice.

Provided the important character of the solution is not lost upon the removal of $2iD(\mathbf{n} \cdot \nabla)\mathbf{z}$, one can solve instead of Eq. (14) the following problem

$$2J(\nabla - i\mathbf{A} - i\kappa\boldsymbol{\sigma})^2 \mathbf{z} + B\sigma_z \mathbf{z} = \lambda\mathbf{z}. \quad (15)$$

We further assume that the fictitious field produced by \mathbf{A} is uniform, and choose the Landau gauge $A_x = 0$, $A_y = -Hx$. The problem of self-consistently deciding the vector potential \mathbf{A} is reduced to that of a single constant H , answering to the first source of non-linearity pointed out earlier. As in the typical Landau level problem we introduce a plane-wave solution for the y -component, $\mathbf{z}(x, y) = e^{iky} \mathbf{z}(x)$, where $\mathbf{z}(x)$ obeys

$$2J(\partial_x - i\kappa\sigma_x)^2 \mathbf{z} - 2J(k + Hx - \kappa\sigma_y)^2 \mathbf{z} + B\sigma_z \mathbf{z} = \lambda\mathbf{z}. \quad (16)$$

We have verified that $H > 0$ corresponds to the (over)screening of the external field B by the induced field H .

Introducing the magnetic length $l_H = 1/\sqrt{H}$, and $x_k = x + kl_H^2$, one can derive the solution of Eq. (16) in the form $z_1 = \phi_n(x_k/l_H)$, $z_2 = id_n \phi_{n+1}(x_k/l_H)$ where ϕ_n is the n -th oscillator wave function and d_n is a coefficient

$$d_n = \frac{2\kappa\sqrt{2H(n+1)}}{H + B/2J + \sqrt{(H + B/2J)^2 + 8(n+1)\kappa^2 H}}. \quad (17)$$

Focusing on the lowest Landau level solution, $n = 0$, the single-particle wave function obtained reads

$$\mathbf{z}(x_k, y) = e^{iky} \begin{pmatrix} \phi_0(x_k/l_H) \\ id_0 \phi_1(x_k/l_H) \end{pmatrix}. \quad (18)$$

Wave functions with different k 's are degenerate, and can be grouped into a linear combination in the manner of Abrikosov solution, Eq. (13):

$$\mathbf{z}_{\text{SkX}} = \left(\frac{2l_x}{(1+d_0^2)l_H\sqrt{\pi}} \right)^{1/2} \times \sum_{j=-\infty}^{\infty} c_j e^{i2\pi jy/l_y} \begin{pmatrix} e^{-x_j^2/(2l_H^2)} \\ id_0 \sqrt{2} x_j e^{-x_j^2/(2l_H^2)} / l_H \end{pmatrix}. \quad (19)$$

Here k is quantized as $k = 2\pi j/l_y$, j =integer, and x_j abbreviates $x + jl_x$. Comparison with the vortex lattice solution shows that l_H serves as the correlation length ξ , as well as the Skyrmion lattice spacing through the condition $l_x l_y = 2\pi l_H^2$. The overall constant reflects the average normalization $(1/\text{Area}) \int dx dy \mathbf{z}^\dagger \mathbf{z} = \langle \mathbf{z}^\dagger \mathbf{z} \rangle = 1$.

We will now show that the state written down in Eq. (19) captures all essential aspects of the Skyrme crystal state. Rather than trying to justify the various approximations that led to Eq. (19), we regard it as a variational state, whose energy can be checked against those of other possible spin states. In this way we can construct a phase diagram similar to the one shown in the previous subsection.

For the triangular array of Skyrmions, c_j is chosen equal to 1 and i for even and odd integers, respectively, and l_y equal to $\sqrt{3} l_x/2$. Energy per area \mathcal{E} evaluated by inserting the variational solution, Eq. (19), into Eq. (5) and carrying out the spatial integration reads

$$\mathcal{E}_{\text{SkX}} = 2J \left(2\kappa^2 - \frac{4\sqrt{2H}\kappa d_0}{1+d_0^2} + \frac{1+3d_0^2}{1+d_0^2} H \right) - B \frac{1-d_0^2}{1+d_0^2}. \quad (20)$$

The extremum condition $\partial \mathcal{E}_{\text{SkX}} / \partial H = 0$ uniquely fixes H , hence the magnetic length l_H . One can read off the relevant energy scales better by dividing out both sides by $4J\kappa^2 = D^2/J$:

$$\begin{aligned} \frac{\mathcal{E}_{\text{SkX}}}{D^2/J} &= 1 - \frac{2\sqrt{2}d_0}{1+d_0^2} \frac{1}{\kappa l_H} + \frac{1+3d_0^2}{1+d_0^2} \frac{1}{2\kappa^2 l_H^2} - b \frac{1-d_0^2}{1+d_0^2}, \\ d_0 &= \frac{2\sqrt{2}\kappa l_H}{1+2\kappa^2 l_H^2 b + \sqrt{(1+2\kappa^2 l_H^2 b)^2 + 8\kappa^2 l_H^2}}. \end{aligned} \quad (21)$$

We used the field in reduced unit $b = B/(D^2/J)$ in the above expressions. The re-scaling makes it clear that the relevant Zeeman energy is indeed D^2/J , in agreement with the analysis of the previous subsection.

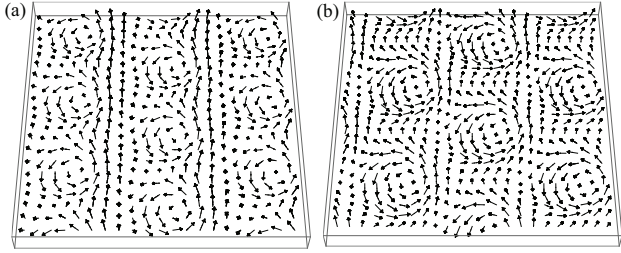


FIG. 5: (color online) (a) A typical Skyrme crystal spin configuration given by Eq. (19) with $B = D^2/J$, with the optimized lattice spacing $\kappa l_H = \sqrt{3}/2$. (b) Skyrme crystal spin configuration obtained by Monte Carlo method from the lattice spin model¹⁰.

Figure 5 (a) shows the typical spin configuration given out by the CP^1 solution \mathbf{z}_{SkX} for $b = 1$ ($B = D^2/J$). Optimizing the energy gives out $\kappa l_H = \sqrt{3}/2$. Spins are pointing up, aligned with the B direction, away from the Skyrminion center and pointing down at the core. The sense of spin swirling (vorticity) in the core region is consistent with the right-handed proper screw direction of the helical spin phase. Reversing the sign of κ , hence $d_0 \rightarrow -d_0$ in Eq. (19), leads to the left-handed screw and a clockwise swirling of spins near the cores. For comparison a typical Skyrme crystal configuration produced from the Monte Carlo annealing of the lattice spin model¹⁰ is reproduced in Fig. 5 (b). It is clear that the essential features of the Skyrminion lattice configuration has survived the several drastic approximations employed in arriving at the Skyrme crystal solution \mathbf{z}_{SkX} .

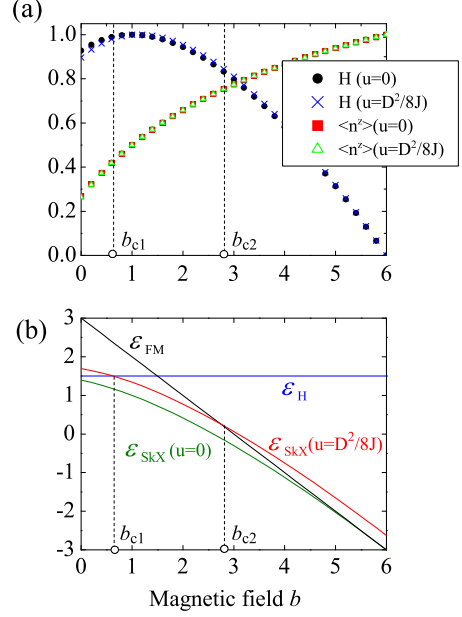


FIG. 6: (color online) (a) Self-consistently induced field H (in the dimensionless unit $\kappa^2 H$) and the ferromagnetic polarization $\langle n^z \rangle$, against external magnetic field $b = B/(D^2/J)$. Taking $\kappa l_H = \sqrt{3}/2$, two different values of u (see text for definition), $u = 0$ and $u = (1/8)(D^2/J)$ were used with little differences in the results. (b) Energies of helical, Skyrme crystal, and ferromagnetic spin states against b , both measured in units of D^2/J . SkX energy \mathcal{E}_{SkX} goes up with u while the other energies remain insensitive to u . b_{c1} and b_{c2} define the two first-order transitions.

Self-consistently determined H and the average polarization $\langle n^z \rangle = \langle \mathbf{z}^\dagger \sigma^z \mathbf{z} \rangle = (1 - d_0^2)/(1 + d_0^2)$ against the external field b are shown in Fig. 6 (a). It is seen that H tends to zero as the external field drives full polarization of spins, $\langle n^z \rangle \approx 1$. The core size and the Skyrminion spacing, both of which are fixed by l_H , diverges accordingly. In reality the divergence is cut off by a first-order transition to the energetically more favorable FM state at the upper critical field B_{c2} .

Shown in Fig. 6 (b) are the energies of the three main competing spin configurations - helical, Skyrme crystal, and ferromagnetic spin states - plotted against b . The SkX state gives the lowest energy regardless of the field strength, in contrast to both Monte Carlo¹⁰ and experimental¹¹ findings showing the ground state evolution helical \rightarrow SkX \rightarrow FM with increasing B . We also find that the energy is insensitive to the crystal structure of the Skyrminions being a square or a triangular lattice.

Both these problems can be remedied by re-visiting the constraint $\mathbf{z}^\dagger \mathbf{z} = 1$, which is so far imposed at the crudest, mean-field level. Helical and FM spin solutions obey the constraint exactly anyway, but the SkX solution does not. An inclusion of the potential term $u(\mathbf{z}^\dagger \mathbf{z} - 1)^2$

($u > 0$) in the free energy density (5), which imposes the constraint at the local level, would increase the energy density of the SkX solution by $u[(\mathbf{z}_{\text{SkX}}^\dagger \mathbf{z}_{\text{SkX}})^2 - 1]$. As seen in Fig. 6 (b), a suitable choice of u restores the correct sequence of ground states punctuated by two critical fields, B_{c1} for helical \rightarrow SkX and B_{c2} for SkX \rightarrow FM transitions. According to Fig. 6 (a), H remains close to unity in the whole SkX region, implying the inter-Skyrmionic spacing l_H comparable to the period of the spin spiral $\lambda \sim \kappa^{-1}$. This is indeed the case both in the Monte Carlo calculation¹⁰ and experimentally^{6,11}. The chance of a larger Skyrmion spacing as H becomes very small is pre-empted by the transition to a ferromagnetic phase with a lower energy at $B = B_{c2}$. Finally, the average $\langle (\mathbf{z}_{\text{SkX}}^\dagger \mathbf{z}_{\text{SkX}})^2 \rangle$ calculated at a number of (B, H, κ) values is in favor of the triangular lattice having a lower energy over the square lattice. This is the same criterion used by Abrikosov¹⁵ and subsequent workers²⁰ in identifying the most stable lattice structure of vortices by calculating the average of $|\psi|^4$ in the U(1) GL theory. Unlike in Abrikosov's case, the average $\langle (\mathbf{z}_{\text{SkX}}^\dagger \mathbf{z}_{\text{SkX}})^2 \rangle$ depends on the (B, H, κ) values used and are not universal.

With \mathbf{z}_{SkX} at hand, the induced field distribution

$$H_{\text{SkX}}(x, y) = i(\partial_x \mathbf{z}_{\text{SkX}}^\dagger \partial_y \mathbf{z}_{\text{SkX}} - \partial_y \mathbf{z}_{\text{SkX}}^\dagger \partial_x \mathbf{z}_{\text{SkX}}) - (2\pi/l_y)(x/l_x) \partial_x (\mathbf{z}_{\text{SkX}}^\dagger \mathbf{z}_{\text{SkX}}) \quad (22)$$

can be worked out²¹. Figure 7 (a) gives the field distribution, along with the distribution of the z -component of the local magnetization $n^z(x, y)$ in Fig. 7 (b). The field intensity reaches a maximum at the Skyrmion core and nearly equals zero in the FM background. The spatial average of $H_{\text{SkX}}(x, y)$ is approximately equal to H used as an input in \mathbf{z}_{SkX} .

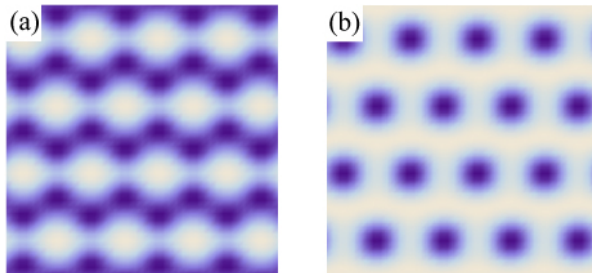


FIG. 7: (color online) (a) Induced field distribution $H_{\text{SkX}}(x, y)$ from the Skyrmion lattice solution \mathbf{z}_{SkX} . Bright area is the Skyrmion core where the intensity is the maximum. (b) Distribution of $n^z(x, y) = \mathbf{z}_{\text{SkX}}^\dagger \sigma^z \mathbf{z}_{\text{SkX}}$. Dark area means reversed spins at the Skyrmion core.

We should emphasize that in the 3D chiral magnets it is the conical phase, with the propagation vector along the \hat{z} -direction, having the lower energy and hence occupying the lower temperature side of the phase diagram instead of the SkX state, under moderate magnetic field⁶⁻⁸. The conical phase cannot exist in a 2D system, and this probably contributes to the SkX state being realized at low

temperature for thin-film samples. It still remains an interesting challenge how one can understand the crossover in the behavior from 2D to 3D systems.

C. Comparison to earlier work

Bogdanov and collaborators have extensively investigated the possibility of the Skyrmion formation in chiral magnets on the basis of Ginzburg-Landau models with Dzyaloshinskii-Moriya interaction^{12,13}. In particular the field dependence of the phase diagram presented in Ref. 13 (Fig. 9 in their paper) correctly captures the spiral \rightarrow SkX \rightarrow FM phase change recently investigated by Monte Carlo method¹⁰, experimentally¹¹, and in the previous two subsections. The analysis of subsection III A amounts to their “circular-cell” approximation.

In Ref. 13 the nature of the phase transition from SkX to FM was not determined conclusively. Based on our analysis presented in Secs. III A and III B, it is clearly first-order. Physically this should be clear since there is no way to turn off topological defects in a continuous fashion. Nor is it possible to fuse a Skyrmion with an anti-Skyrmion to annihilate them, since the system under consideration consists only of one species of Skyrmions^{6-8,10,11}. Experiments also support the first-order phase boundary¹¹.

In their analysis, Bogdanov *et al.* assumed a two-dimensional structure homogeneously extended along the third direction. Our model is explicitly two-dimensional. With the recent experimental input⁶ we know that for known 3D chiral magnets such as MnSi, in the field range where the SkX phase (a.k.a. A-phase) is found, the low-temperature state has the conical spin structure. In order to stabilize the Skyrmionic phase it is therefore essential to suppress the three-dimensionality as well as to turn on a magnetic field. The present investigation fills in the gap that existed between the early theoretical work and the new insights offered by recent experimental progress.

Finally, our paper presents a new framework for dealing with chiral magnetic systems. The CP^1 formulation allows us to understand the Skyrmion lattice formation in direct analogy to the Abrikosov vortex problem in superconductors, and to the Landau-level physics. It is our belief that the new formulation can be used in conjunction with the conventional classical vector theory in studying other aspects of chiral magnetism such as their dynamics.

IV. DISCUSSION

Although the detailed examination of the thermal effects at nonzero temperature is outside the scope of this paper, we can make qualitative assessment about the thermal fluctuations for the Skyrme crystal state. Both translational and spin rotational symmetries are broken in the SkX state, and one accordingly expects two

types of Goldstone modes: phonon-like displacements of Skyrmion positions and spin waves.

Applying the Lindemann criterion, the melting of the Skyrmion lattice will take place if the thermal fluctuation in the center-of-mass position of a Skyrmion becomes comparable to the inter-Skyrmion spacing. As discussed in the previous section, the typical magnetic energy difference per spin for the three magnetic phases - helical, SkX, and FM - are of the order D^2/J . A shift of the Skyrmion position by one lattice unit increases the energy per spin by a typical amount D^2/J , or Jl_H^{-2} if the linear size of the Skyrmion $l_H \sim \kappa^{-1} \sim J/D$ is used. The energy increase associated with the Skyrmion displacement by x should then be $J \times (x/l_H)^2$. Applying the equipartition theorem we obtain $J \times \langle x^2 \rangle / l_H^2 \sim T$ at a temperature T , and the melting temperature $T_m \sim J$ from the condition $\sqrt{\langle x^2 \rangle} \sim l_H$.

Another possible disordering mechanism is the spin fluctuation. In the ground state each Skyrmion unit cell exhibits identical spin configuration. If the spin orientation of one particular Skyrmion unit cell is completely reversed, the cost in Zeeman energy is roughly B times the number of spins, or Bl_H^2 . Noting that B in the relevant SkX phase is D^2/J , we conclude that the single-Skyrmion spin flip has the energetic cost of J . From this we conclude that the coupling energy of adjacent Skyrmions must be $J \times (\Delta\theta/\pi)^2$ for a small angle difference $\Delta\theta$ of the two nearby Skyrmion spin orientations. By invoking equipartition theorem again, we arrive at a spin-melting temperature $T_m \sim J$. In conclusion, destroying the global ordering of the SkX state by either center-of-mass displacement or spin fluctuation requires a temperature of order J , even though the magnetic field energy difference between the various phases is only D^2/J . It is the large size of the Skyrmion, of order $(J/D)^2$, which compensates for the small magnetic energy scale and renders a sizable melting temperature.

To summarize, we have provided a theoretical treat-

ment of the Skyrme crystal phase recently observed in the thin film of chiral magnet $\text{Fe}_{0.5}\text{Co}_{0.5}\text{Si}^{11}$. Two independent constructions of the Skyrmion lattice state were used to calculate the energy of this state and compare it against those of other competing states, namely helical spin and ferromagnetic spin, as the perpendicular magnetic field strength is increased. The resulting phase diagram giving the successive ground state evolution of helical \rightarrow SkX \rightarrow FM phases is in accord with the Monte Carlo simulation¹⁰ and the thin-film experiment¹¹. We gave a general argument for the two critical field strengths separating the SkX state from the helical state on the low-field side and from the FM state on the high-field side to be of order D^2/J . Other spiral magnets with similar spin structures are expected to exhibit Skyrme crystal phase for field ranges of D^2/J if they are made in the thin-film form. We also gave a qualitative argument why the melting of the Skyrme crystal should occur at $T_m \sim J$ despite the small magnetic energy scale D^2/J needed to stabilize the SkX phase. As an interesting by-product, we derived the variational wave function corresponding to the Skyrme crystal state in the CP^1 form.

Acknowledgments

N. N. is supported by Grant-in-Aids for Scientific Research (No. 17105002, 19019004, 19048008, 19048015, and 21244053) from the Ministry of Education, Culture, Sports, Science and Technology of Japan, and also by Funding Program for World-Leading Innovative R&D on Science and Technology (FIRST Program). H. J. H. is supported by Mid-career Researcher Program through NRF grant funded by the MEST (No. R01-2008-000-20586-0), and in part by the Asia Pacific Center for Theoretical Physics.

-
- ¹ T. H. R. Skyrme, Proc. Roy. Soc. (London) A **260**, 127 (1961); Nuc. Phys. **31**, 556 (1962).
 - ² S. L. Sondhi, A. Karlhede, S. A. Kivelson, and E. H. Rezayi, Phys. Rev. B **47**, 16419 (1993).
 - ³ S. E. Barrett, G. Dabbagh, L. N. Pfeiffer, K. W. West, and R. Tycko, Phys. Rev. Lett. **74**, 5112 (1995); E. H. Aifer, B. B. Goldberg, and D. A. Broido, Phys. Rev. Lett. **76**, 680 (1996); V. F. Mitrović, M. Horvatić, C. Berthier, S. A. Lyon, and M. Shayegan, Phys. Rev. B **76**, 115335 (2007).
 - ⁴ L. Brey, H. A. Fertig, R. Côté, and A. H. MacDonald, Phys. Rev. Lett. **75**, 2562 (1995).
 - ⁵ G. Gervais, H. L. Stormer, D. C. Tsui, P. L. Kuhns, W. G. Moulton, A. P. Reyes, L. N. Pfeiffer, K. W. Baldwin, and K. W. West, Phys. Rev. Lett. **94**, 196803 (2005); Yann Gallais, Jun Yan, Aron Pinczuk, Loren N. Pfeiffer, and Ken W. West, Phys. Rev. Lett. **100**, 086806 (2008); Han Zhu, G. Sambandamurthy, Yong P. Chen, P. Jiang, L. W. Engel, D. C. Tsui, L. N. Pfeiffer, and K. W. West, Phys.

- Rev. Lett. **104**, 226801 (2010).
- ⁶ S. Mühlbauer, B. Binz, F. Joinetz, C. Pfleiderer, A. Rosch, A. Neubauer, R. Georgii, and P. Böni, Science **323**, 915 (2009).
- ⁷ W. Munzer, A. Neubauer, T. Adams, S. Mühlbauer, C. Franz, F. Jonietz, R. Georgii, P. Boni, B. Pedersen, M. Schmidt, A. Rosch, and C. Pfleiderer, Phys. Rev. B **81**, 041203(R) (2010).
- ⁸ C. Pfleiderer, T. Adams, A. Bauer, W. Biberacher, B. Binz, F. Birkelbach, P. Böni, C. Franz, R. Georgii, M. Janoschek, F. Jonietz, T. Keller, R. Ritz, S. Mühlbauer, W. Münzer, A. Neubauer, B. Pedersen, and A. Rosch, J. Phys.:Condens. Matter **22**, 164207 (2010).
- ⁹ A. Neubauer, C. Pfleiderer, B. Binz, A. Rosch, R. Ritz, P. G. Niklowitz, and P. Böni, Phys. Rev. Lett. **102**, 186602 (2009).
- ¹⁰ Su Do Yi, Shigeki Onoda, Naoto Nagaosa, and Jung Hoon Han, Phys. Rev. B **80**, 054416 (2009).

- ¹¹ X. Z. Yu, Y. Onose, N. Kanazawa, J. H. Park, J. H. Han, Y. Matsui, N. Nagaosa, and Y. Tokura, *Nature (London)* **465**, 901 (2010).
- ¹² A. N. Bogdanov and D. A. Yablonskii, *Sov. Phys. JETP* **68**, 101 (1989).
- ¹³ A. Bogdanov and A. Hubert, *J. Magn. Magn. Mater.* **138**, 255 (1994).
- ¹⁴ Per Bak and M. Høgh Jensen, *J. Phys. C* **13**, L881 (1980).
- ¹⁵ A. A. Abrikosov, *Sov. Phys. JETP* **5**, 1174 (1957).
- ¹⁶ A. Tonomura, H. Kasai, O. Kamimura, T. Matsuda, K. Harada, Y. Nakayama, J. Shimoyama, K. Kishio, T. Hanaguri, K. Kitazawa, M. Sasase and S. Okayasu, *Nature* **412**, 620 (2001).
- ¹⁷ N. Nagaosa, *Quantum Field Theory in Strongly Correlated Electronic Systems*, Chap. 5 (Springer, 1999).
- ¹⁸ It is instructive to note that the original analysis of Skyrme (Ref. 1) was carried out in the language which amounts to what we call the CP¹ formulation.
- ¹⁹ R. Rajaraman, *Solitons and Instantons*, Chap. 3 (North Holland, 1987).
- ²⁰ W. H. Kleiner, L. M. Roth, and S. H. Autler, *Phys. Rev.* **133**, A1226 (1964).
- ²¹ The $(2\pi/l_y)(x/l_x)\partial_x(\mathbf{z}_{\text{SkX}}^\dagger \mathbf{z}_{\text{SkX}})$ restores the lattice translational invariance of $H_{\text{SkX}}(x, y)$ and would be unnecessary if the constraint $\mathbf{z}^\dagger \mathbf{z} = 1$ was obeyed exactly.